

Impacts of Land-Use Data on the Simulation of Surface Air Temperature in Northwest China

Yaohui LI¹, Cailing ZHAO^{1*}, Tiejun ZHANG¹, Wei WANG¹, Haixia DUAN¹,
Yuanpu LIU¹, Yulong REN¹, and Zhaoxia PU²

¹ Key Laboratory for Arid Climate Change and Disaster Reduction of Gansu Province, Lanzhou Institute of Arid Meteorology/
Northwestern Regional Center of Numerical Weather Prediction, Key Open Laboratory for Arid Climate Change and
Disaster Reduction of the China Meteorological Administration, Lanzhou 730000, China

² Department of Atmospheric Sciences, University of Utah, UT 84112, USA

(Received May 21, 2018; in final form August 7, 2018)

ABSTRACT

This study examines the impacts of land-use data on the simulation of surface air temperature in Northwest China by the Weather Research and Forecasting (WRF) model. International Geosphere–Biosphere Program (IGBP) land-use data with 500-m spatial resolution are generated from Moderate Resolution Imaging Spectroradiometer (MODIS) satellite products. These data are used to replace the default U.S. Geological Survey (USGS) land-use data in the WRF model. Based on the data recorded by national basic meteorological observing stations in Northwest China, results are compared and evaluated. It is found that replacing the default USGS land-use data in the WRF model with the IGBP data improves the ability of the model to simulate surface air temperature in Northwest China in July and December 2015. Errors in the simulated daytime surface air temperature are reduced, while the results vary between seasons. There is some variation in the degree and range of impacts of land-use data on surface air temperature among seasons. Using the IGBP data, the simulated daytime surface air temperature in July 2015 improves at a relatively small number of stations, but to a relatively large degree; whereas the simulation of daytime surface air temperature in December 2015 improves at almost all stations, but only to a relatively small degree (within 1°C). Mitigation of daytime surface air temperature overestimation in July 2015 is influenced mainly by the change in ground heat flux. The modification of underestimated temperature comes mainly from the improvement of simulated net radiation in December 2015.

Key words: surface air temperature, land-use data, numerical simulation, Northwest China

Citation: Li, Y. H., C. L. Zhao, T. J. Zhang, et al., 2018: Impacts of land-use data on the simulation of surface air temperature in Northwest China. *J. Meteor. Res.*, **32**(6), 896–908, doi: 10.1007/s13351-018-7151-5.

1. Introduction

Land-use is a very important parameter in atmospheric numerical models. Different land-use categories have different physical properties, and they can change the energy balance and vertical fluxes of moisture, heat and momentum between soil and air, which determine the calculation of meteorological variables such as air temperature near the surface (Jiménez-Esteve et al., 2018).

Land-use categories indicate whether a region is covered by forests, cropland, or water, as well as human

land uses, such as urban areas. The accuracy of a land-use dataset influences the simulation of land surface processes. Presently, the default land-use dataset used in the Weather Research and Forecasting (WRF) model is the U.S. Geological Survey (USGS) dataset with a spatial resolution of about 1 km. It was generated from satellite images acquired between April 1992 and March 1993. Because the USGS dataset used in China has not been recently updated, it is unable to accurately reflect the land-use conditions of some regions, such as urban areas (Weng, 2002; Sertel et al., 2010; Schicker et al., 2016).

Supported by the China Meteorological Administration Special Public Welfare Research Fund (GYHY201506001) and National Natural Science Foundation of China (41675015).

*Corresponding author: zhaocl@iamcma.cn.

©The Chinese Meteorological Society and Springer-Verlag Berlin Heidelberg 2018

Different land-use datasets determine the parameters used in the calculation of surface heat fluxes in land surface models. Some researchers have studied the impacts of land-use change on weather and climate change using mesoscale weather and climate models (Gao et al., 2003; Xu et al., 2015). Recently, it has been demonstrated that different land-use data can significantly affect numerical simulations. Qu et al. (2013) investigated the impacts of urbanization and the reduction of farmland area on the air temperature across the North China Plain with 1 km resolution land-use data, showing that urbanization led to an increase of 0.03°C per year in this area. The surface air temperature varied significantly with the land-use categories. The impacts of the accuracy of land-use data on model simulations have also been examined (Cheng and Byun, 2008; De Noblet-Ducoudré et al., 2012). Santos-Alamillos et al. (2015) investigated the effects of land-use change on climate through simulations and observations. Cheng et al. (2013) have shown that the land-use dataset in the WRF model was unable to accurately represent the actual land-use distribution in Taiwan. In addition, the impacts of a land-use dataset generated from remote sensing data in 2007 on the simulation of air temperature and wind speed were analyzed. The results showed that the use of an accurate dataset could reduce both the underestimation of air temperature and the overestimation of wind speed in the WRF model. Sertel et al. (2010) studied the impacts of land-use dataset (with 1-km resolution) quality on regional climate simulation and found that accurate representation of land cover is essential for climate simulations because the land surface controls the distribution of energy and water. Pielke et al. (2011) studied the effects of surface changes with 1-km spatial resolution dataset on simulations of regional climate, showing that snow, precipitation, and vegetation distribution were well matched by improving the accuracy of the land-use dataset. The accuracy of the land-use dataset was also very important in climate models. De Meij and Vinuesa (2014) suggested that after replacing the land-use dataset in the WRF model with the 2006 Corine dataset at 100-m resolution, the simulations of temperature, wind speed, and precipitation were all improved to some degree. In Europe, the spatial resolution of the more-recent Corine land-use dataset is 100 m. However, at present, the spatial resolutions of most available land-use datasets are coarser than 1 km.

Northwest China is located in arid Central Asia and is affected by the East Asian monsoon. It has a dry–wet climate and ecosystem transitions with relatively intense land–atmosphere interactions. Moreover, Northwest China has complex terrain and underlying surfaces as

well as sparse vegetation, so it has relatively intense climate change and land–atmosphere interactions. Therefore, further study is needed to ascertain whether surface air temperature simulations in Northwest China are more sensitive to the impacts of land-use data.

In this study, using Moderate Resolution Imaging Spectroradiometer (MODIS) satellite products, we first generate a new land-use dataset (with 500-m spatial resolution) that has a finer spatial resolution than the default land-use dataset (about 1-km spatial resolution) in the WRF model. This new dataset is employed in the WRF model to explore the impacts of land-use data on the simulation of surface air temperature. Then, the effects of the updated land-use dataset on the simulation of surface air temperature are analyzed. Finally, the reasons for the differences between the surface air temperature simulations are discussed. Our objective in this study is to provide a basis for improving simulations of surface air temperature over complex terrain in Northwest China.

This paper is organized as follows. The model and the experiment design are described in Section 2, and the land-use data processing is described in Section 3. The simulation results, including statistical analyses of land-use data, are included in Section 4. Finally, Section 5 provides a brief discussion and a summary of the relevant results.

2. Model description and experiment design

2.1 Description of the WRF model

The WRF-ARW Version 3.6.1 model is used in this study. The WRF model is a new-generation mesoscale forecasting model and assimilation system developed by scientists from US research departments and universities. WRF is a fully compressible non-hydrostatic model with a horizontal lattice Arakawa-C format, a vertical coordinate system of power quality, and a Euler center based on terrain following. Physical parameterization schemes can be selected in the model, including microphysics, cumulus, planetary boundary layer, and land surface processes.

The WRF model includes the WRF Pre-Processing System (WPS), the WRF model, and the WRF Data Assimilation (WRFDA) and post-processing systems. The WPS contains the initial data used to define the simulation domain, interpolate the terrestrial data (including ground vegetation, terrain, soil type, land-use, etc.), and horizontally interpolate the initial data into the simulation domains.

2.2 Experiment design

In this study, the $0.5^\circ \times 0.5^\circ$ GFS (Global Forecast Sys-

tem) data (<http://www.nco.ncep.noaa.gov/pmb/products/gfs/>) from NCEP are used to provide the boundary and initial conditions, and the simulation is on three nested domains. Boundary conditions are forced every 3 hours. The center of the simulation is set to 39°N, 100°E. The settings of the test parameters are shown in Table 1, and the simulation domain is shown in Fig. 1. The model utilizes the terrain-following mass η coordinates. It is vertically divided into 40 layers with 50 hPa at the top. The parameterization schemes of physical processes are as follows: the microphysics scheme is the Thompson scheme, the planetary boundary layer scheme is ACM2, the longwave scheme is the RRTM (Rapid Radiative Transfer Model) scheme, the shortwave scheme is the Dudhia scheme, and the cumulus parameterization is the KF scheme in D01 and D02 (there is no cumulus parameterization in D03). The land surface scheme in this study is the Noah land surface mode, which becomes increasingly important because the WRF model needs to capture mesoscale circulations forced by surface variability in albedo, land-use, and snow.

The Noah land surface model is a unified NCEP/NCAR/AFWA scheme with soil temperature and moisture in four layers (10, 30, 60, and 100 cm thick), and with one layer of snow lumped with the top soil layer. The vegetation is one vegetation type in each grid cell without the dynamic vegetation and carbon budget (Ek et al., 2003; Jin et al., 2010). Together with the land sur-

face model, the surface layer scheme computes the stability-dependent coefficients and permits a calculation of the surface turbulent fluxes for the planetary boundary layer scheme. These prognostic states are provided by WPS. The control file contains model configuration variables such as the number and thickness of soil layers, number and length of time steps, initial date/time of the simulation, location of the simulation site, initial conditions for all state variables, and site-specific land classifications (integer indexes for vegetation type, soil type, and surface slope type).

In this study, the model simulates 48 h starting every day, and the results for D03 are output per hour. Because the results from 48 h are obtained every day, the spin-up time is set as the first 12 hours of the results.

2.3 Data processing method

A variety of statistical methods are available for surface air temperature evaluation. In this study, the following statistical methods for error analysis are used:

$$ME = \frac{1}{n} \sum_{i=1}^n (F_i - O_i),$$

$$RMSE = \sqrt{\frac{1}{n} \sum_{i=1}^n (F_i - O_i)^2}.$$

where n is the number of samples (specifically, n is the number of observation stations), F_i is the simulation result for station i , and O_i is the observation made at station i .

The mean error (ME) represents the mean difference between the simulated values for all observation stations and the corresponding observed values. The root-mean-square error (RMSE) represents the square root of the ratio of the summed squared deviations of the simulated values for all observation stations and the corresponding observed values relative to the number of observation stations (n).

3. Data processing

3.1 Land-use data processing

The default land-use data in the WRF model are taken from the USGS land-use dataset, which was generated a long time ago, such that the representativeness of this dataset has gradually dwindled over time. The land-use categories have obviously changed under climate change and human activities in recent years (Jiang et al., 2008; Grossman-Clarke et al., 2010).

In this study, a new land-use dataset is generated based on land survey data for China from 2000 to 2005.

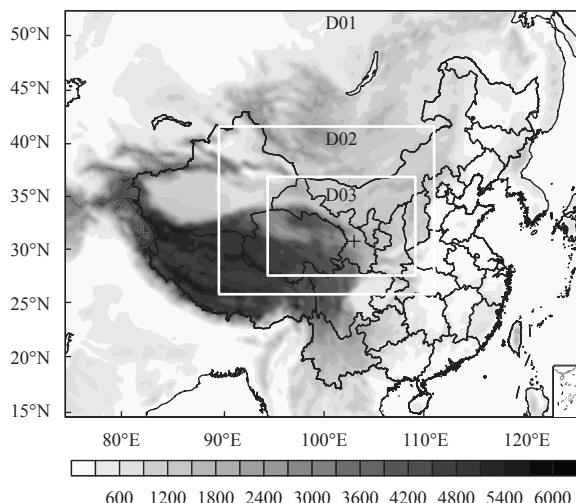


Fig. 1. Simulation domains (D01, D02, and D03) used in the model with terrain height (shading; m)

Then, the relatively high-accuracy MODIS (Moderate Resolution Imaging Spectroradiometer) products and IGBP (International Geosphere–Biosphere Program) land-use dataset are integrated by using GIS (Geographic Information System) for spatial analysis and a discrimination algorithm. In addition, integrated land classification data are processed by using MODIS water-mask products to determine whether the land categories are correct. Finally, a land-use product (<http://westdc.westgis.ac.cn/>) is generated with 500-m spatial resolution, which is finer than that of most recently available land-use datasets. The method of land-use data processing is provided by Ran et al. (2009, 2010), and the accuracy of the new dataset has been verified; the IGBP land-use dataset has good labeling accuracy (Wang et al., 2013; Wu et al.,

2013).

The default USGS land-use dataset in the WRF model is classified into 24 types, whereas the new IGBP land-use dataset derived from remote sensing data is classified into 17 types. In order to facilitate the comparison of the USGS and IGBP land-use datasets, the USGS dataset is reclassified by using the IGBP land-use dataset classification method (Qu et al., 2013). Figures 2a and 2b show the distributions of the reclassified USGS land-use dataset and the IGBP land-use dataset over D03. The index illustrates the dominant land-use category of each grid point, and the main land-use changes in D03 from the USGS dataset to the IGBP dataset are presented in Fig. 2c.

Compared to the USGS dataset, the IGBP land-use

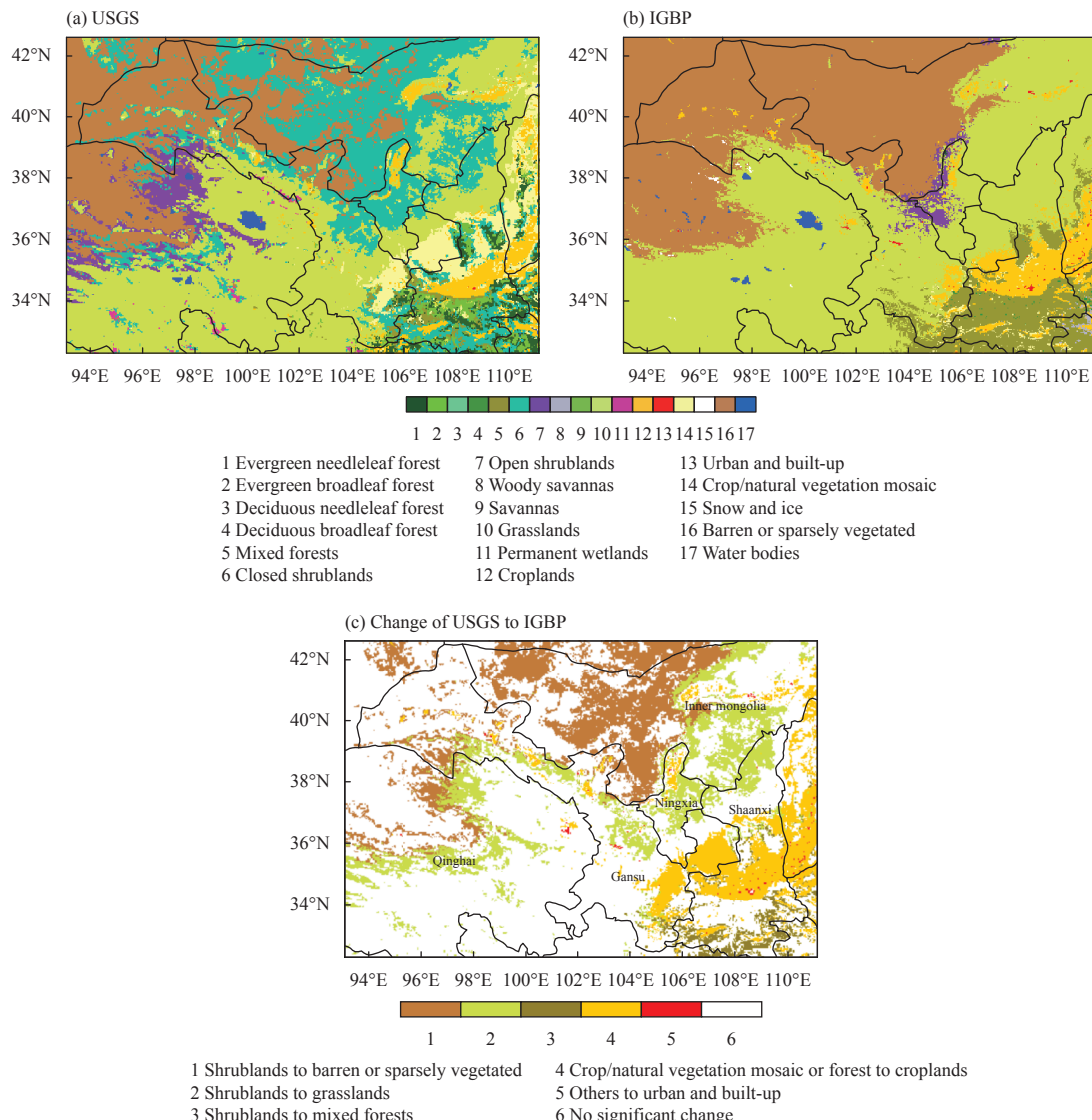


Fig. 2. Dominant land-use index of each grid in D03 at 3-km resolution from the (a) USGS and (b) IGBP land-use datasets, and (c) major land-use changes from the USGS to IGBP datasets in D03. The names of the provinces in D03 are shown in (c).

dataset shows some significant changes (Fig. 2c). The main differences are in western Inner Mongolia and northwestern Qinghai, with land-use types varying from shrublands to barren or sparsely vegetated. In addition, land-use types in Ningxia and eastern Gansu Province change from shrublands to grassland, and from forest and crop/natural vegetation mosaic to cropland, respectively. Some relatively small areas change to mixed forests from shrublands. Some fragments of urban and built-up areas appear in Northwest China.

Table 3 shows the parameters of different land-use categories in the WRF model, as well as the numbers of cells (last two columns) occupied by different land-use categories in D03. It clearly exhibits the characteristics and distribution ranges of different land-use categories in D03. Compared with the USGS land-use dataset, the IGBP dataset shows significantly smaller areas of shrublands, deciduous broadleaf forest, tropical savanna, farmland, and vegetation mosaic. To some extent, a smaller water body area is also revealed in the IGBP dataset. Relatively larger areas of mixed forest, grassland, and urban centers are presented, as well as slightly larger areas of ice/snow and desert. These results are consistent with the conclusions documented by Wang et al. (2017) regarding changes in farmland, forest land, and grassland in China.

3.2 Observation data

Hourly surface air temperatures observed by national

basic meteorological observing stations in Northwest China are utilized to evaluate the simulated results. The observation data have been verified by checking the climatological threshold value, regional threshold value, time consistency, and spatial consistency.

4. Results

4.1 Comparison of differences in the simulation of daily daytime surface air temperature

Simulation of nighttime surface air temperature is largely affected by boundary layer processes. The WRF model produces relatively larger errors in the evolution of the nighttime boundary layer. To more clearly compare the impacts of different land-use datasets on surface air temperature simulation in the WRF model, 12-h (0800–2000 BT) daytime surface air temperature simulation results are used for the analyses in this study. In order to ensure the unity of the simulation results, the time used in this study is Beijing Time (BT).

Figure 3 shows the simulated results from the 168 stations that have different land-use categories in the USGS and IGBP land-use datasets. These results can more clearly illustrate the impacts of land-use datasets on the simulated surface air temperature.

Specifically, Fig. 3 compares the observed and simulated average daily daytime (ADD), lowest daily daytime (LDD), and highest daily daytime (HDD) surface air temperature values from 168 stations in July 2015. A comparison of the ADD surface air temperature (Fig. 3a) shows that the replacement of the USGS dataset by the IGBP dataset can mitigate the overestimation of temperature. Simulated LDD surface air temperature based on the IGBP land-use data is closer to observations (Fig.

Table 2. Simulation test schemes

Test	Test period	Land-use data used in the WRF model
Test 1 (T1)	2015.7.1–7.31 & 2015.12.1–12.31	USGS
Test 2 (T2)	2015.7.1–7.31 & 2015.12.1–12.31	IGBP

Table 3. Corresponding properties of land-use classification in the model and the number of cells in the simulated region

Value	Land-use type	Albedo	Z_0 (m)	SHDFAC	R_s (m^{-1})	Cells in the USGS	Cells in the IGBP
1	Evergreen needleleaf forest	0.10	1.09	0.7	125	4	63
2	Evergreen broadleaf forest	0.11	2.65	0.95	150	1	0
3	Deciduous needleleaf forest	0.11	0.85	0.7	150	39	0
4	Deciduous broadleaf forest	0.12	0.80	0.8	100	4782	172
5	Mixed forests	0.12	0.80	0.8	125	2286	16,946
6	Closed shrublands	0.25	0.03	0.7	300	49,630	34
7	Open shrublands	0.23	0.05	0.7	170	8315	2692
8	Woody savannas	0.2	0.86	0.5	70	0	397
9	Savannas	0.2	0.86	0.5	70	3478	1
10	Grasslands	0.19	0.08	0.8	40	74,594	101,779
11	Permanent wetlands	0.12	0.04	0.6	40	27	7
12	Croplands	0.17	0.07	0.8	40	7989	10,950
13	Urban and built-up	0.15	1.00	0.1	200	30	334
14	Crop/natural vegetation mosaic	0.19	0.07	0.8	40	10,662	1076
15	Snow and ice	0.0	0.001	0	999	1	152
16	Barren or sparsely vegetated	0.12	0.01	0.01	999	46,867	74,914
17	Water bodies	0.19	0.00	0	100	2286	859

SHDFAC represents model variable for vegetation fraction, and R_s represents stomatal resistance.

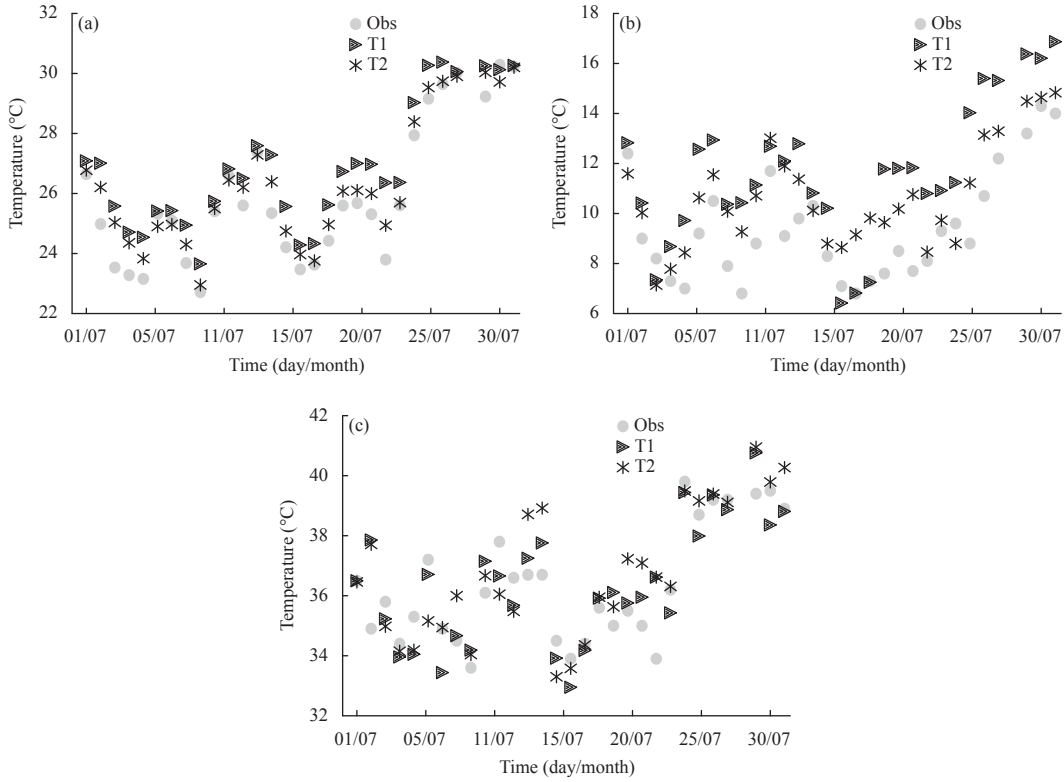


Fig. 3. Comparison of simulated (a) daily average, (b) minimum, and (c) maximum surface air temperature in July 2015. These are the average results from 168 stations that have different land-use categories in the USGS and IGBP land-use datasets.

3b). However, the simulation of HDD surface air temperature using the IGBP land-use data is not significantly improved for most days (Fig. 3c). The LDD of T1 and the ADD and LDD of T2 reach the 0.05 significance level. Therefore, improvement in the simulated daytime surface air temperature in July 2015 using the IGBP land-use dataset comes mainly from the improvement in LDD surface air temperature simulation.

Figure 4 compares the observed and simulated ADD, LDD, and HDD surface air temperature of T1 and T2 in December 2015. Similar to the results in July 2015, the ADD simulation results in T2 are closer to the observations (Fig. 4a) than those in T1. Compared with observations, the simulated ADD surface air temperature in T1 is more underestimated than that in T2. Using the IGBP land-use data can significantly mitigate the underestimated simulated temperature, particularly for days after 14 December 2015. Although the simulation of the LDD surface air temperature is not considerably improved in T2 (Fig. 4b), some simulation results are closer to the observations than in T1. Compared with the simulated LDD surface air temperature, T1 mitigates the underestimated simulated HDD surface air temperature significantly (Fig. 4c). The ADD and HDD of T1 and T2 reach the 0.05 significance level. Therefore, the improvement in

the simulation in daytime surface air temperature in December 2015 in T2 comes mainly from the improvement in HDD surface air temperature simulation.

The simulated surface air temperature in July and December 2015 shows that replacement of the USGS dataset by the IGBP land-use dataset can improve the simulation of the ADD surface air temperature during these two months, but to varying degrees. The use of the IGBP land-use dataset more significantly improves the simulation of the LDD surface air temperature in July 2015 and the HDD surface air temperature in December 2015.

Table 4 shows that the RMSEs between the simulations and observations in July and December 2015 are similar to those in Figs. 3 and 4. Using the IGBP land-use dataset can more significantly improve the simulation of the ADD surface air temperature in December 2015 (by 39%) compared to the use of the USGS land-use data. The RMSE (0.46) for the simulated LDD surface air temperature based on the USGS land-use data is greater than that based on the IGBP land-use data (0.27) in July 2015. Moreover, the RMSE (0.45) for the simulated HDD surface air temperature in December 2015 based on the USGS land-use data is greater than that based on the IGBP land-use data (0.36). However, com-

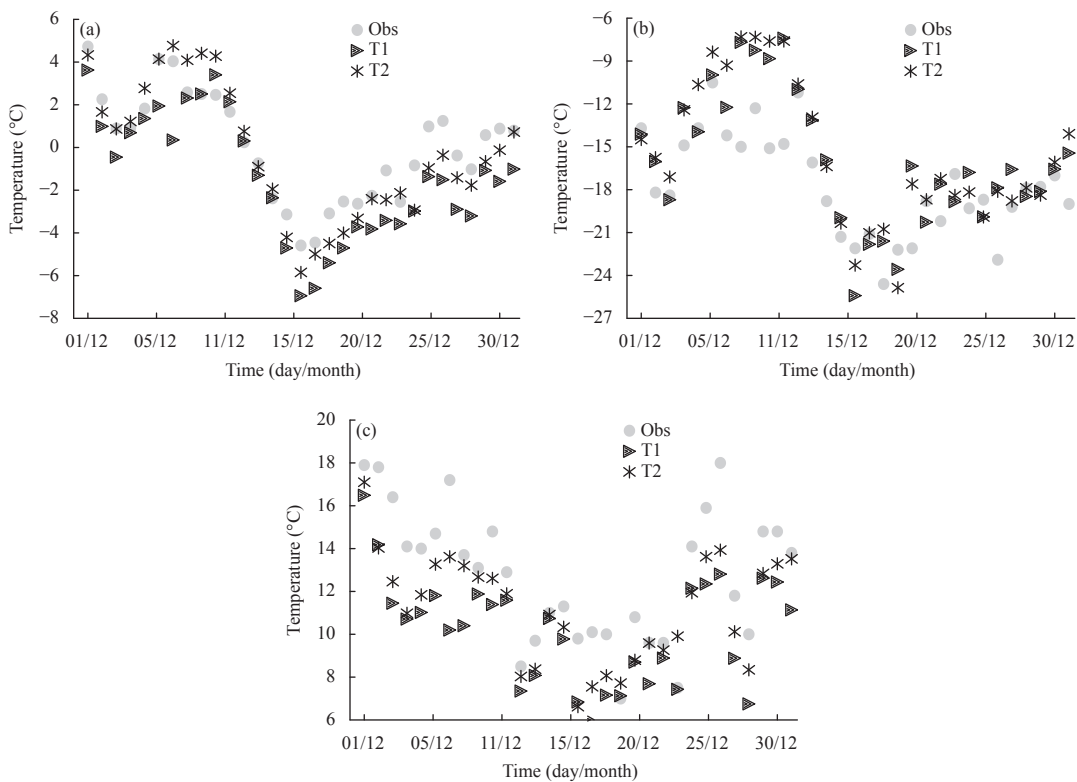


Fig. 4. As in Fig. 3, but for December 2015.

Table 4. RMSEs between simulations and observations (T&O) of T1 and T2 (average, minimum, and maximum surface air temperature)

Time	T_{avg}		T_{min}		T_{max}	
	T1&O	T2&O	T1&O	T2&O	T1&O	T2&O
2015.07	0.20*	0.11	0.46*	0.24*	0.18	0.21
2015.12	0.26*	0.14*	0.41	0.43	0.45*	0.34*

Note: * trends significant at $p = 0.05$

pared with the USGS land-use data, the use of the IGBP land-use data results in higher RMSEs for both the simulated HDD surface air temperature in July 2015 and the simulated LDD surface air temperature in December 2015. The relevant factors behind this phenomenon require further study.

4.2 Comparison of regional distribution

Figures 5a and 5b show the spatial distribution of the errors in T1 and T2 in July 2015, respectively. It is clear that the errors in T1 are predominantly positive. As demonstrated in Fig. 5b, the errors in the simulated ADD surface air temperature of the observation stations in Gansu based on the IGBP land-use data are relatively small in T2, compared with those in T1. The errors of some stations in northwest Gansu are in the range of [2, 3] to [1, 2]. In addition, the errors of most stations in central Gansu are in the range of [-1, 1], which are lower than those in T1. The largest simulation errors of the Shaanxi Province are located mainly in the central re-

gion, with the largest errors exceeding 2°C. No significant improvement appears in the simulated ADD surface air temperature for the stations in Shaanxi in T2. The relatively large errors of some stations in T1 are reduced in T2 in Qinghai.

Because positive and negative errors cannot be easily compared, absolute errors are used in the following section to comparatively analyze the simulation results based on the USGS and IGBP land-use datasets.

The difference in the distribution of the absolute errors in the simulated ADD surface air temperature in D03 is shown in Fig. 5c, which more clearly exhibits the differences between the simulated results based on the USGS and IGBP land-use data. Specifically, each result in Fig. 5c is computed by subtracting the absolute error of the simulated ADD surface air temperature based on the USGS land-use dataset and the observation at the corresponding station from the corresponding absolute error of the simulated ADD surface air temperature based on the IGBP land-use data and the observation at the corres-

ponding station. The positive value (red dot) indicates that the absolute error in T1 is greater than that in T2. In addition, the larger difference between the absolute errors in T1 and T2 shows that the simulation is improved more significantly by using the IGBP land-use data. The negative value (blue dot) indicates that the absolute error in the simulated ADD surface air temperature based on the IGBP land-use data is greater than that based on the USGS land-use data.

A total of 286 stations with observation data in July 2015 are selected after data quality control. As demonstrated in Fig. 5c, using the IGBP land-use dataset improves the simulations for 144 stations and leads to an increase in the absolute error for 142 stations compared with the results in T1.

Figures 6a and 6b present the spatial distribution of the errors in the simulated ADD surface air temperature in December 2015 for T1 and T2. In contrast to July 2015, the errors of most stations in D03 in December 2015 are predominantly positive. As demonstrated in Fig. 6c, the simulated surface air temperature values in December 2015 based on the IGBP land-use data are higher than those simulated based on the USGS land-use data. Thus, negative errors for relevant stations in T1 are reduced by applying the IGBP land-use dataset, as in the stations in central Gansu, southern Ningxia, northern Shaanxi, and the juncture of Qinghai and Gansu.

However, positive errors for relevant stations in T1 increase when using the IGBP land-use data. In particular, positive errors for the stations in central Shaanxi in T1 significantly increase when the IGBP land-use data are applied.

The distribution of these stations indicates that the differences between the absolute errors in the simulated ADD surface air temperature in July 2015 for the stations in central and northwest Gansu based on the USGS and IGBP land-use datasets are predominantly positive. This suggests that the use of the IGBP land-use data can significantly improve the simulation of the ADD surface air temperature compared with T1 (with improvement generally exceeding 2°C). This further indicates that the results of T2 over these stations present a significant improvement.

Compared with July 2015, the overall distribution of the differences shows that the use of the IGBP land-use data more significantly improves the simulation of surface air temperature in December 2015. Within D03, using the IGBP land-use data improves the simulation for 205 stations (positive values; red dots in Fig. 6) and leads to an increase in the absolute error for 81 stations (negative values; blue dots in Fig. 6).

The distribution of the stations in different regions shows that the use of the IGBP land-use dataset significantly improves the simulated ADD surface air temperat-

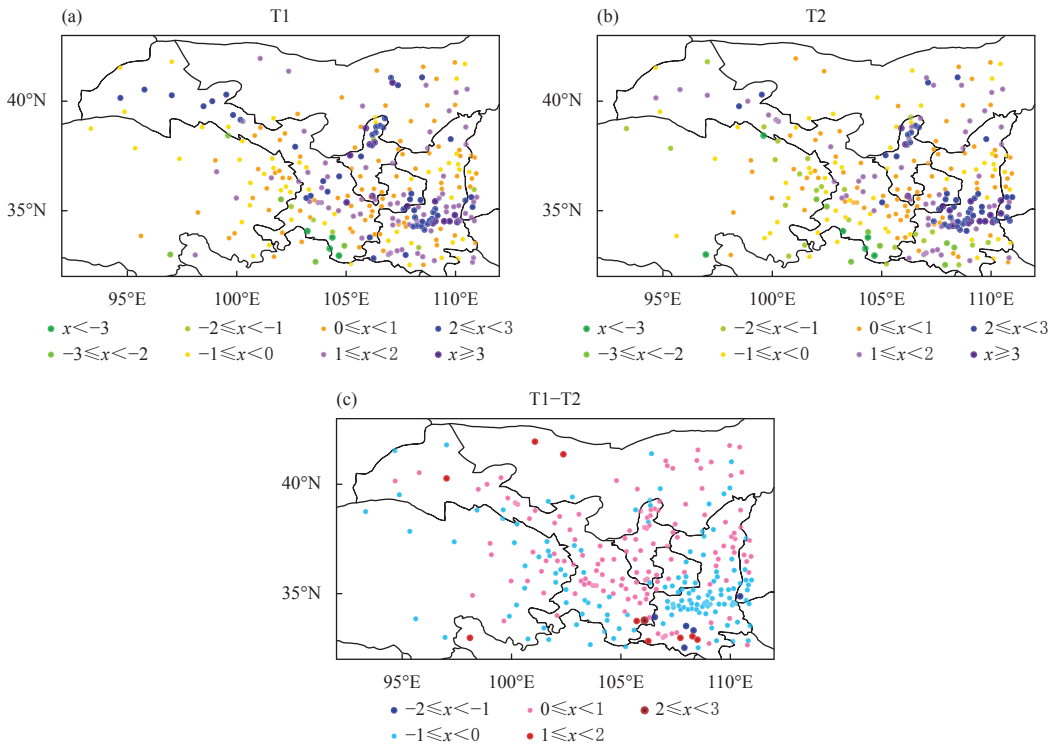


Fig. 5. Spatial distributions of errors and the difference in absolute error (T1–T2) in D03 in July 2015. (a) T1, (b) T2, and (c) T1–T2.

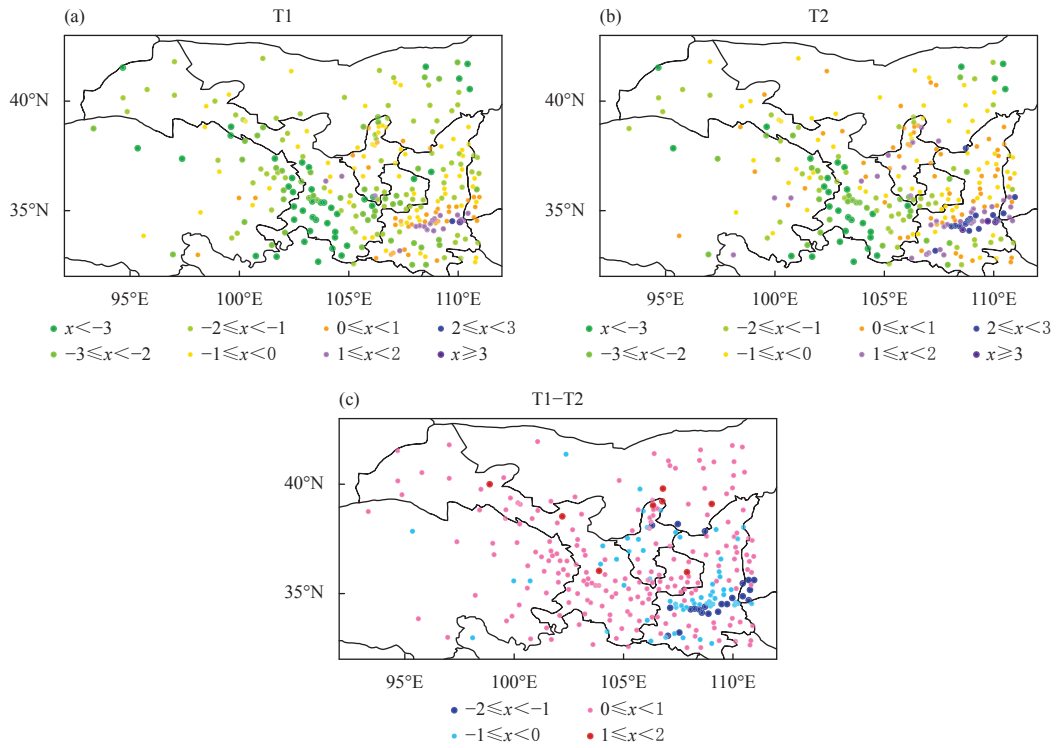


Fig. 6. As in Fig. 5, but for December 2015.

ure for nearly all stations in Gansu except an extremely small number of stations, for which the use of the IGBP land-use data leads to an increase in the absolute error.

A comparison of the differences between the absolute errors indicates that the use of the IGBP land-use data improves the simulation for more stations in December 2015 than in July 2015, although the improvements are relatively small (0–1°C). Overall, using the IGBP land-use data improves the model's skill in simulating surface air temperature in Northwest China.

4.3 Impacts of land-surface parameters on surface air temperature

Updated land-use data can directly alter relevant surface parameters, including surface albedo, leaf area index, and surface roughness. These variations can further induce changes in the radiation flux of the land surface and can consequently change the surface air temperature. These parameters can influence the calculation of surface heat and moisture fluxes in land-surface models. Changing the land-use data will directly alter these surface properties in the model, resulting in changes in the surface air temperature simulation (Krayenhoff and Voogt, 2010).

Figure 7 illustrates the relevant surface parameters affected by the land-use dataset in July 2015. The parameters in December 2015 are similar (figure omitted). Com-

pared to T1, the southeast and northwest portions of D03 present lower surface albedo in T2. Other parameters are larger in T2, and it exhibits opposite results in D03. The results of the evaluation are more influenced by simulations in the northwest portions of D03 because more observation sites are located in this area.

Solar radiation is the most fundamental source of land-atmosphere system energy. Figure 8 shows the ground heat flux, sensible heat flux, latent heat flux, and net radiation of T1 and T2. The results are the mean values from 168 stations that have differences in the USGS and IGBP land-use data. This clearly suggests the impacts of changing the land-use dataset on the simulated results.

A comparison of the ground heat flux (GRDFLX) between T1 and T2 in July 2015 is shown in Fig. 8a. It can be seen that the GRDFLX values for T1 and T2 are negative. A comparison of surface air temperature and GRDFLX is consistent with this. Since LDD is influenced largely by GRDFLX, the improvement in LDD in July 2015 may come mainly from the improvement in GRDFLX. From the comparison between Figs. 8g and 8h, and Figs. 4 and 5, it is noted that the net radiation is consistent with the daily maximum surface air temperature. The improvement in December 2015 may come mainly from the correction of net radiation. Higher thermal inertia (Fig. 7e) suggests that lower temperature

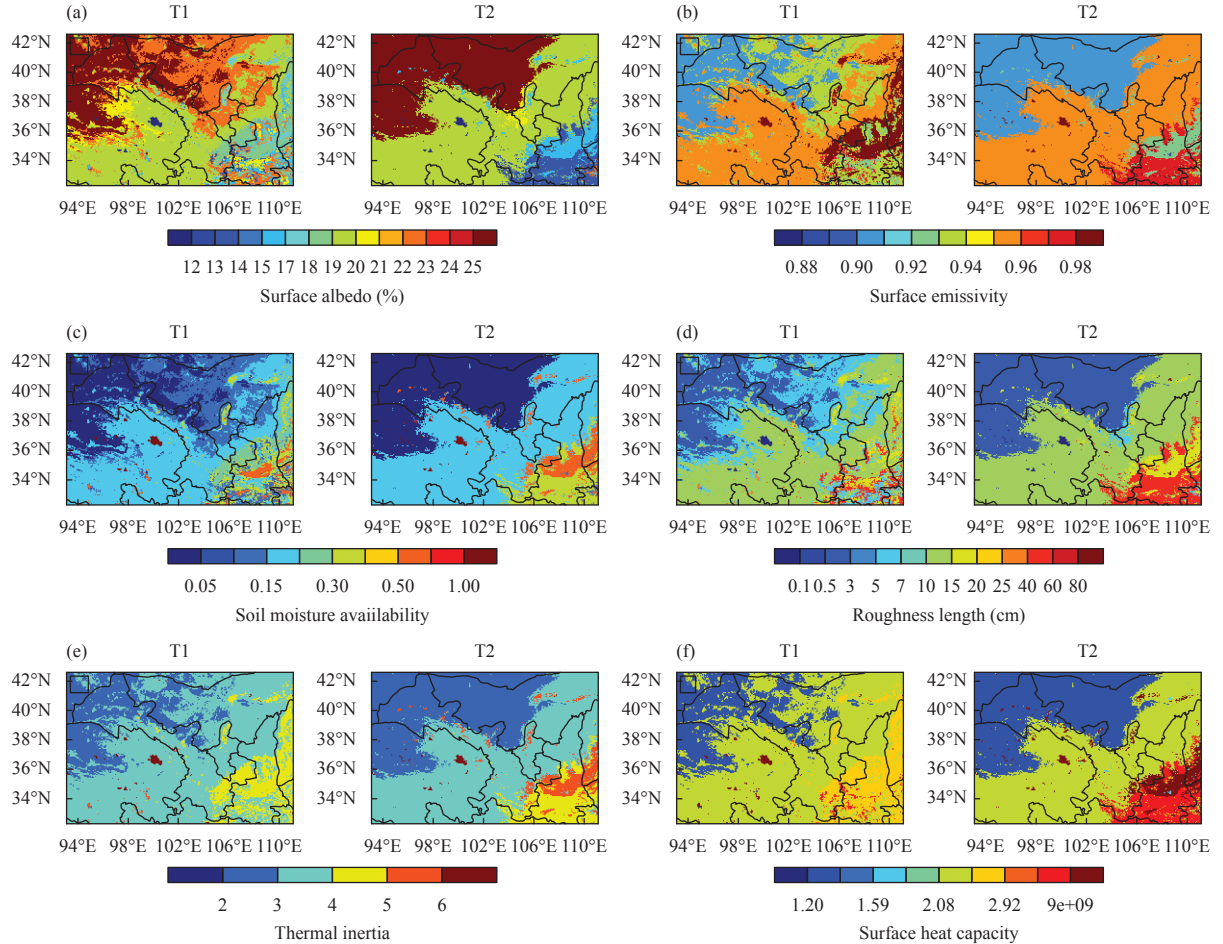


Fig. 7. Spatial distributions of the 6 main physical parameters for T1 and T2 over D03 in July 2015: (a) surface albedo (%), (b) surface emissivity, (c) soil moisture availability, (d) roughness length (cm), (e) thermal inertia, and (f) surface heat capacity.

will be reached in T2 compared with T1. The increased urbanization in T2 will also modify the physical properties. Lower surface albedo (Fig. 7a) can generate larger net radiation.

A comparison of SH and LH is coincident with that of the surface air temperature. It should be noted that the change is not exactly the same as the flux change, because the factors influencing surface air temperature are more complex.

Figure 9 shows the changes in surface radiation and energy budgets after the major land-use data change from the USGS to IGBP datasets over D03. The results are the average results of these grid cells of different categories as indicated in Fig. 2. The changes in the LDD surface air temperature are affected largely by GRDFLX. Compared with the observations in July 2015 (Fig. 3b), the simulations significantly overestimate the LLD. The GRDFLX in T2 is smaller than that in T1 in the major land-use change categories (categories 1, 2, and 3). Although urbanization (category 5) exhibits significantly larger GRDFLX, the degree of influence is quite limited

because the area is much smaller than the others. By improving the overestimation of GRDFLX in T2, LDD is also improved.

Compared to LDD, NET can largely influence HDD. Both T1 and T2 underestimate HDD in December 2015. Using the IGBP land-use dataset simulates larger NET in most areas (categories 2, 3, 4, and 5). Due to the correction of NET at the surface in T2, the underestimation of HDD is also modified. Higher thermal inertia (Fig. 7e) and lower surface albedo (Fig. 7a) modify the overestimation of LDD in July 2015 and the underestimation of HDD in December 2015. Moreover, the simulation skill of surface air temperature is improved by using IGBP data. The results of these areas are consistent with the averaged results for the 168 stations.

5. Conclusions and discussion

In this study, the impacts of the finer spatial resolution (500 m) IGBP land-use dataset and the default USGS land-use dataset on the simulations of surface air

temperature are compared in Northwest China. Simulations of surface air temperature with a spatial resolution of 3 km in July and December 2015 are evaluated. The

accuracy of the simulated surface air temperature is examined by comparing it with observations from the basic national observation stations in Northwest China. The

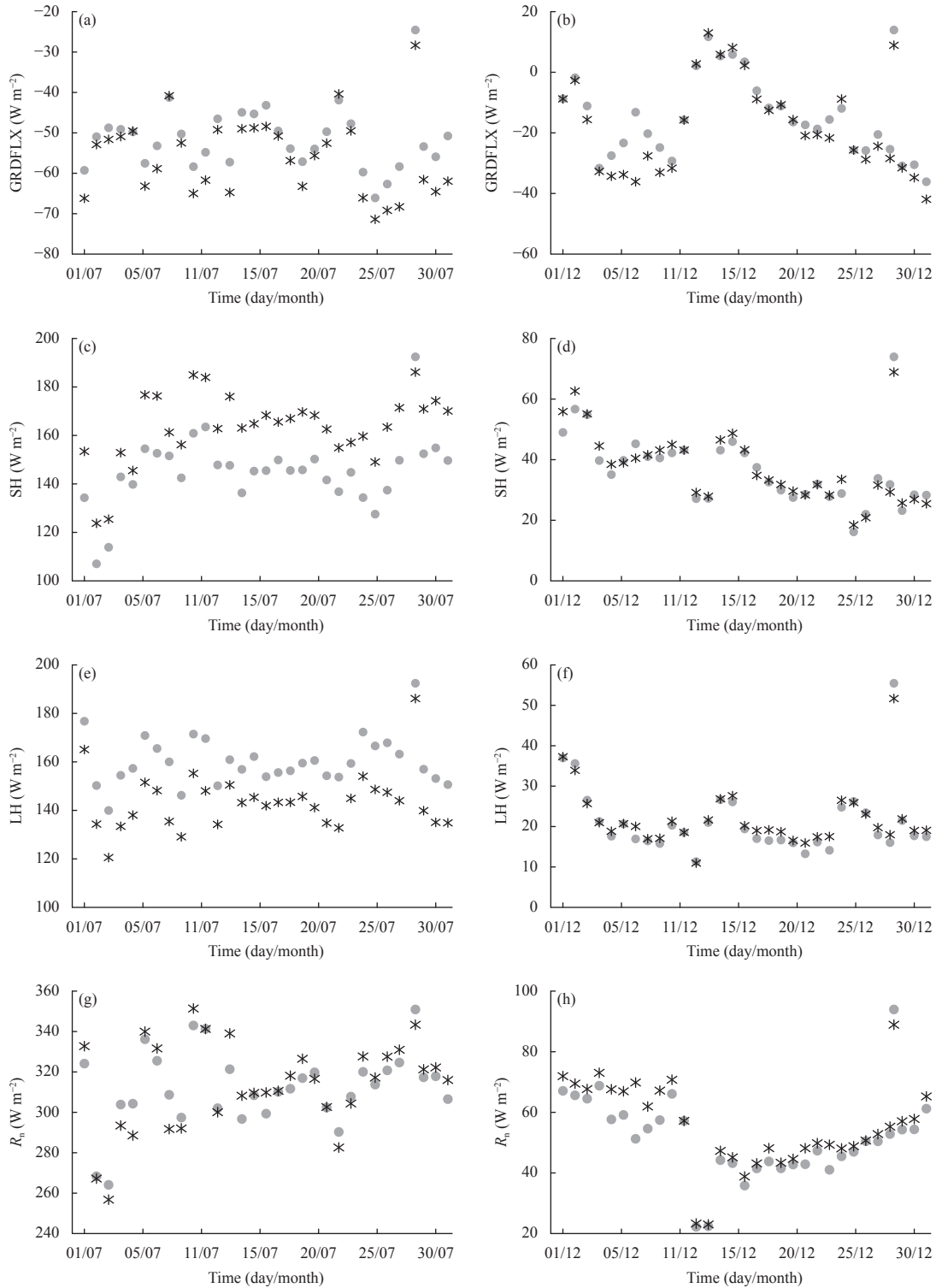


Fig. 8. (a, b) Comparisons of ground heat flux (GRDFLX), (c, d) sensible heat flux (SH), (e, f) latent heat flux (LH), and (g, h) net radiation (R_n) in (a, c, e, g) July 2015 and (b, d, f, h) December 2015. These results are the average results from 168 stations that have differences in the USGS and IGBP land-use data.

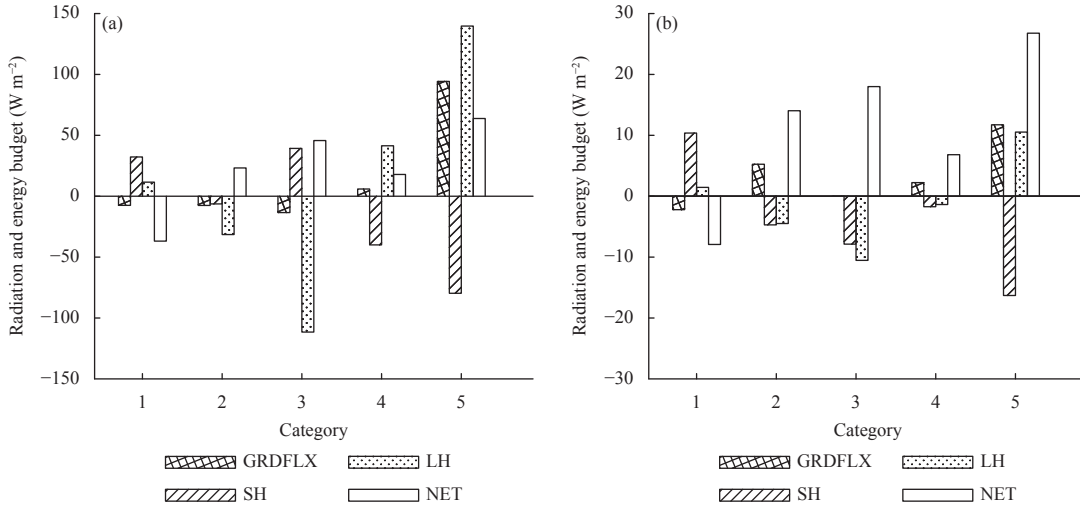


Fig. 9. Differences (T2–T1) in average surface radiation and energy budget of major land-use change from the USGS to IGBP datasets for (a) July and (b) December 2015 in D03. The categories shown here are the same as those in Fig. 2c. 1: shrublands to barren or sparsely vegetated, 2: shrublands to grasslands, 3: shrublands to mixed forests, 4: crop/natural mosaic or forest to croplands, and 5: others to urban and built-up.

main conclusions are summarized below.

We first generate a new land-use dataset (IGBP land-use dataset) derived from MODIS satellite products. Compared with the default USGS data in the WRF model, the IGBP data can more accurately illustrate the increase in desert, grassland, and urban areas, as well as the decrease in closed shrublands areas in Northwest China.

The impacts of different land-use datasets on the simulation of surface air temperature are evaluated. Replacing the default USGS land-use data with the IGBP data improves the simulation of surface air temperature in Northwest China in both July and December 2015, although to varying degrees in different seasons. The distribution of errors varies between seasons (July and December 2015). Overall, the use of the new land-use data improves the simulation results and can enhance the model's skill in simulating surface air temperature in Northwest China.

In each grid cell, the various land-use categories determine the local radiative and energy balances, which further affect the sensible and latent heat fluxes. Local surface air temperature is sensitive to the different categories of land-use. Mitigation of the lowest daily daytime surface air temperature overestimation is due mainly to the improved ground heat flux in July 2015. Modification of the underestimation of the highest daily daytime surface air temperature simulation may come mainly from the improvement of net radiation in December 2015.

Different land-use types vary significantly in physical, chemical, and biological processes, resulting in large differences in the surface energy balance and water balance.

Different types of land-uses have different impacts on local climate change. Because the error of the WRF model in the simulation of surface air temperature varies between seasons, surface air temperature is simulated in two typical months in this study. Further simulations of the surface air temperature in different seasons is needed to verify the simulation results over larger time scales. Spatial resolution has a large impact on whether land-use conditions can be accurately represented. Therefore, future work will focus on further examination of the impacts of spatial resolution in order to find the resolution that can most accurately represent land-use conditions.

Acknowledgment. We thank the two anonymous reviewers and the editor-in-chief for their comments to improve this paper.

REFERENCES

- Cheng, F.-Y., and D. W. Byun, 2008: Application of high resolution land use and land cover data for atmospheric modeling in the Houston–Galveston metropolitan area. Part I: Meteorological simulation results. *Atmos. Environ.*, **42**, 7795–7811, doi: 10.1016/j.atmosenv.2008.04.055.
- Cheng, F.-Y., Y.-C. Hsu, P.-L. Lin, et al., 2013: Investigation of the effects of different land use and land cover patterns on mesoscale meteorological simulations in the Taiwan area. *J. Appl. Meteor. Climatol.*, **52**, 570–587, doi: 10.1175/JAMC-D-12-0109.1.
- De Meij, A., and J. F. Vinuesa, 2014: Impact of SRTM and Corine Land Cover data on meteorological parameters using WRF. *Atmos. Res.*, **143**, 351–370, doi: 10.1016/j.atmosres.2014.03.004.
- De Noblet-Ducoudré, N., J.-P. Boisier, A. Pitman, et al., 2012: Determining robust impacts of land-use-induced land cover changes on surface climate over North America and Eurasia:

- Results from the first set of LUCID experiments. *J. Climate*, **25**, 3261–3281, doi: 10.1175/JCLI-D-11-00338.1.
- Ek, M. B., K. E. Mitchell, Y. Lin, et al., 2003: Implementation of Noah land surface model advances in the National Centers for Environmental Prediction operational mesoscale Eta model. *J. Geophys. Res. Atmos.*, **108**, 8851, doi: 10.1029/2002JD003296.
- Gao, X. J., Y. Luo, W. T. Lin, et al., 2003: Simulation of effects of land use change on climate in China by a regional climate model. *Adv. Atmos. Sci.*, **20**, 583–592, doi: 10.1007/BF02915501.
- Grossman-Clarke, S., J. A. Zehnder, T. Loridan, et al., 2010: Contribution of land use changes to near-surface air temperatures during recent summer extreme heat events in the Phoenix metropolitan area. *J. Appl. Meteor. Climatol.*, **49**, 1649–1664, doi: 10.1175/2010JAMC2362.1.
- Jiang, X. Y., C. Wiedinmyer, F. Chen, et al., 2008: Predicted impacts of climate and land use change on surface ozone in the Houston, Texas, area. *J. Geophys. Res. Atmos.*, **113**, D20312, doi: 10.1029/2008JD009820.
- Jiménez-Esteve, B., M. Udina, M. R. Soler, et al., 2018: Land use and topography influence in a complex terrain area: A high resolution mesoscale modelling study over the Eastern Pyrenees using the WRF model. *Atmos. Res.*, **202**, 49–62, doi: 10.1016/j.atmosres.2017.11.012.
- Jin, J. M., N. L. Miller, and N. Schlegel, 2010: Sensitivity study of four land surface schemes in the WRF model. *Adv. Meteor.*, **2010**, 167436, doi: 10.1155/2010/167436.
- Krayenhoff, E. S., and J. A. Voogt, 2010: Impacts of urban albedo increase on local air temperature at daily–annual time scales: Model results and synthesis of previous work. *J. Appl. Meteor. Climatol.*, **49**, 1634–1648, doi: 10.1175/2010JAMC2356.1.
- Pielke, R. A., A. Pitman, D. Niyogi, et al., 2011: Land use/land cover changes and climate: Modeling analysis and observational evidence. *WIREs: Climate Change*, **2**, 828–850, doi: 10.1002/wcc.144.
- Qu, R. J., X. L. Cui, H. M. Yan, et al., 2013: Impacts of land cover change on the near-surface temperature in the North China Plain. *Adv. Meteor.*, **2013**, 409302, doi: 10.1155/2013/409302.
- Ran, Y. H., X. Li, and L. Lu, 2009: China land cover classification at 1 km spatial resolution based on a multi-source data fusion approach. *Adv. Earth Sci.*, **24**, 192–203, doi: 10.3321/j.issn:1001-8166.2009.02.009. (in Chinese)
- Ran, Y. H., X. Li, and L. Lu, 2010: Evaluation of four remote sensing based land cover products over China. *Int. J. Remote Sens.*, **31**, 391–401, doi: 10.1080/01431160902893451.
- Santos-Alamillos, F. J., D. Pozo-Vázquez, J. A. Ruiz-Arias, et al., 2015: Influence of land-use misrepresentation on the accuracy of WRF wind estimates: Evaluation of GLCC and CORINE land-use maps in southern Spain. *Atmos. Res.*, **157**, 17–28, doi: 10.1016/j.atmosres.2015.01.006.
- Schicker, I., D. A. Arias, and P. Seibert, 2016: Influences of updated land-use datasets on WRF simulations for two Austrian regions. *Meteor. Atmos. Phys.*, **128**, 279–301, doi: 10.1007/s00703-015-0416-y.
- Sertel, E., A. Robock, and C. Ormeci, 2010: Impacts of land cover data quality on regional climate simulations. *Int. J. Climatol.*, **30**, 1942–1953, doi: 10.1002/joc.2036.
- Wang, H. J., S. P. Dai, and X. B. Huang, 2013: The remote sensing monitoring analysis based on object-oriented classification method. *Advances in Image and Graphics Technologies*, T. Tan, Q. Ruan, X. Chen, et al., Eds., Springer, Berlin, Heidelberg, 363, 92–101, doi: 10.1007/978-3-642-37149-3_12.
- Wang, Z., W. D. Yan, S. G. Liu, et al., 2017: Spatial-temporal characteristics of three main land-use types in China based on MODIS data. *Acta Ecologica Sinica*, **37**, 3295–3301, doi: 10.5846/stxb201603010354. (in Chinese)
- Weng, Q. H., 2002: Land use change analysis in the Zhujiang Delta of China using satellite remote sensing, GIS and stochastic modelling. *J. Environ. Manage.*, **64**, 273–284, doi: 10.1006/jema.2001.0509.
- Wu, F., J. Y. Zhan, H. M. Yan, et al., 2013: Land cover mapping based on multisource spatial data mining approach for climate simulation: A case study in the farming–pastoral ecotone of North China. *Adv. Meteor.*, **2013**, 520803, doi: 10.1155/2013/520803.
- Xu, Z. F., R. Mahmood, Z.-L. Yang, et al., 2015: Investigating diurnal and seasonal climatic response to land use and land cover change over monsoon Asia with the community earth system model. *J. Geophys. Res. Atmos.*, **120**, 1137–1152, doi: 10.1002/2014JD022479.